A Second-Order Kinetic Model for Global Analysis of Vibrational Polariton Dynamics

Haochuan Mao[a], Wei Xiong[*a,b]

AFFILIATIONS

[a]Department of Chemistry and Biochemistry, University of California, San Diego, 9500 Gilman Drive, MC 0358, La Jolla, California 92093-0358, United States

[b]Material Science and Engineering Program, University of California, San Diego, 9500 Gilman Drive, MC 0418, La Jolla, California 92093-0418, United States

Corresponding Author *E-mail: w2xiong@ucsd.edu.

Abstract

The interaction between cavity photons and molecular vibrations leads to the formation of vibrational polaritons, which have demonstrated the ability to influence chemical reactivity and change material characteristics. Although ultrafast spectroscopy has been extensively applied to study vibrational polaritons, the nonlinear relationship between signal and quantum state population complicates the analysis of their kinetics. Here, we employ a second-order kinetic model and transform matrix method (TMM), to develop an effective model to capture the nonlinear relationship between the 2D IR (or pump-probe) signal and excited state populations. We test this method on two types of kinetics: a sequential relaxation from the first to the second excited states of dark modes, and a Raman state relaxing into the first excited state. By globally fitting the simulated data, we demonstrate accurate extraction of relaxation rates and ability to identify intermediate species by comparing the species spectra with theoretical ground truth, validating our

method. This study demonstrates the efficacy of a second-order TMM approximation in capturing essential spectral features with up to 10% excited state population, simplifying global analysis and enabling straightforward extraction of kinetic parameters, thus empowering our methodology in understanding of excited-state dynamics in polariton systems.

Introduction

Vibrational polaritons are quasiparticles that emerge from the collective strong coupling between molecular vibrations and cavity modes, which exhibit characteristics of both matter and light. [1-4] These entities have received significant interests from the chemistry community due to their potential to modify ground-state chemical reactions,[5-8] influence photophysical processes within vibrational excited states[9-13] and serve as platforms for quantum information science.[14-16] Despite their promising applications, a few key questions remain unanswered. For instance, it is unclear how polariton states, with lifetimes spanning only several picoseconds, can influence reactions that unfold over minutes to hours,[17-20] or what role is played by the dark states that predominate in most systems.[21, 22]

To understand energy redistributions inside of polaritons and their associated dark states, ultrafast spectroscopy, including pump-probe and two-dimensional (2D) spectroscopy, across visible or infrared spectra,[7, 10, 11, 22-29] has been developed for investigating these processes in polaritonic systems. Using these techniques, it has been demonstrated that vibrational polaritons could alter ultrafast processes in the excited states with time scales of several picoseconds, such as energy relaxation[9, 10] and transfer,[12] polariton propagation, and ultrafast structural isomerization.[13] In these investigations, the primary utility of these techniques is to delineate the population dynamics of intermediate states following photoexcitation, providing insights into how polaritons may alter photophysical behaviors.

Data from pump-probe and 2D spectroscopy are often depicted as two- or three-dimensional arrays, $\Delta S(\boldsymbol{\omega}, t)$, capturing spectral evolution over time at various frequencies $\boldsymbol{\omega}$. This format allows for one-dimensional representation in pump-probe experiments and two-dimensional in 2D spectroscopy at each time delay *t*. For regular molecular species, the various spectral features can be directly related to the population of intermediate states, such as ground state bleach, stimulated emission and excited state/photoinduced absorptions, whose spectral amplitudes are used to track the population dynamics, e.g. following Beer's law.[30] In this case, the decay time constants extract from multi-exponential fitting directly represent the population dynamics of these states.

This approach encounters some challenges when quantifying polariton dynamics. For example, Figure 1 shows the calculated pump-probe spectra and their intensity as a function of the population at given frequencies. If we only consider Rabi-splitting contraction – the reduction of the collective coupling strength due to a decrease of the ground-state population of the molecular modes,[9, 11, 23] the pump-probe spectra are reminiscent of a pair of out-of-phase derivatives of the Lorentzian functions whose line shape remains unchanged but amplitude varies when the change of the ground state population is perturbative (Figure 1a and 1b). Moreover, pump-probe intensities of the derivative spectra and ground state population follow a linear relationship, allowing for the use of peak intensity to represent the ground state population changes (Figure 1c).

Alternatively, to follow the dynamics of the excited states of the dark modes, it is a common practice to follow its absorptive feature , due to its large spectral intensity.[11, 31] In vibrational strong coupling (VSC) systems, after polariton relax to the excited states of dark reservoir modes, the absorption of the excited states of dark modes (in particular the first excited states) often overlaps with the LP transmission window – rendering a large signal amplitude in the pump-probe spectra (Figure 1d and 1e). However, this is where a potential issue lies. As shown in Figure 1f, the

negative feature at the LP region only exhibits a linear increase when the excited state population is below 4%, and overall increases nonlinearly as the population of the first-excited state increases. This nonlinear dependence shows not only in pump-probe transmission spectra, but also in reflection and absorption spectra (Figure 2), which poses challenges to obtain correct time constants from the raw data using simple exponential fitting.

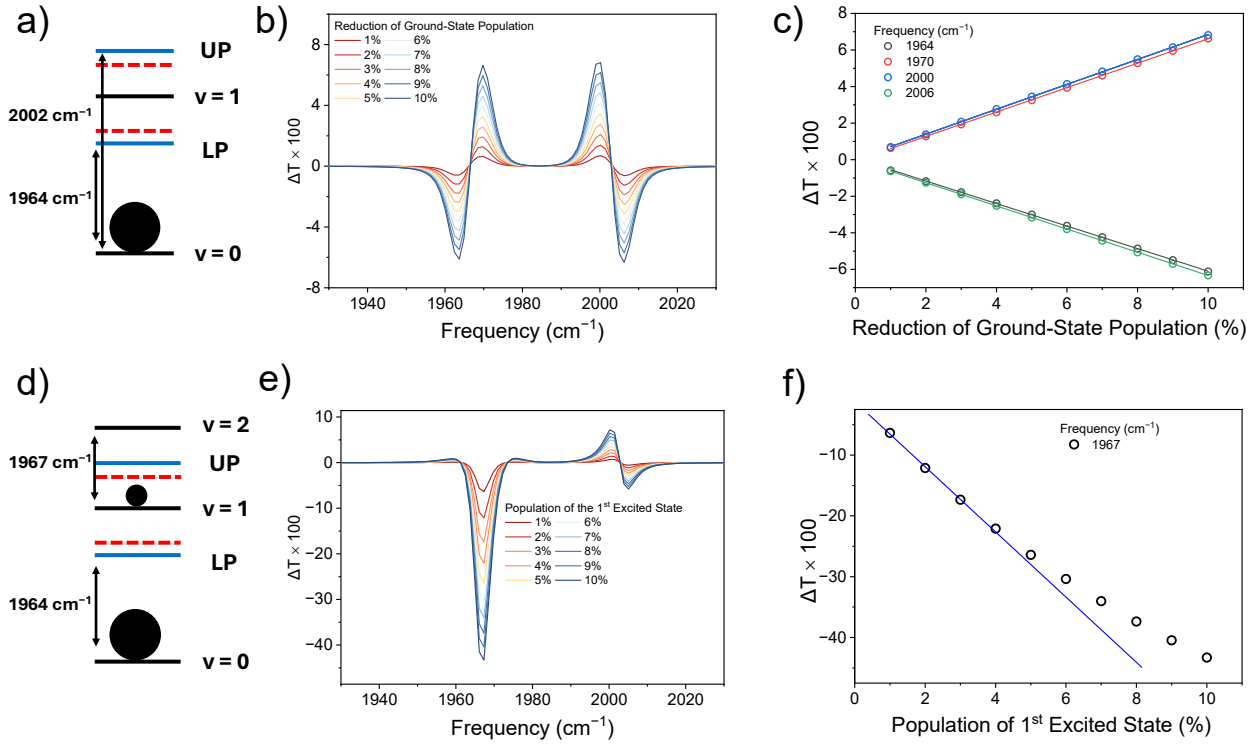

Figure 1: Simulated pump-probe spectra of a Lorentzian oscillator with ground-state frequency of 1983 cm^{-1} that is coupled to the cavity mode. (a) schematic of a two-level system showing Rabi splitting under VSC, and Rabi contraction (red dotted levels). (b) pump probe spectra of a two-level system. (c) population dependence of the signal intensities at given frequencies for (b). (d) schematic of a three-level system with 2←1 overlapping with LP. (e) pump probe spectra of a three-level system with the excited state absorption of 2←1 at 1968 cm^{-1}. (f) Population dependence of the signal intensities at given frequencies for (e)

To resolve this challenge, researchers often apply the model derived from the transform matrix method (TMM) to extract population of the excited and ground states.[9, 32, 33] In this method, the linear polariton spectra at ground and excited states are simulated by TMM, respectively, whose difference is used to fit the pump-probe spectra at a specific time *t*. The populations at *t* can be extracted from the fitting; then the same procedure is repeated at other time delays to obtain the dynamics. Finally, the lifetime of the excited and ground states can be attained by multiexponential fittings. Although widely used,[9, 32, 34] due to its two-step nature, the accuracy of the time constants heavily depends on the quality of the spectral fitting and thereby often requires high quality spectra, in order to retrieve subtle features.

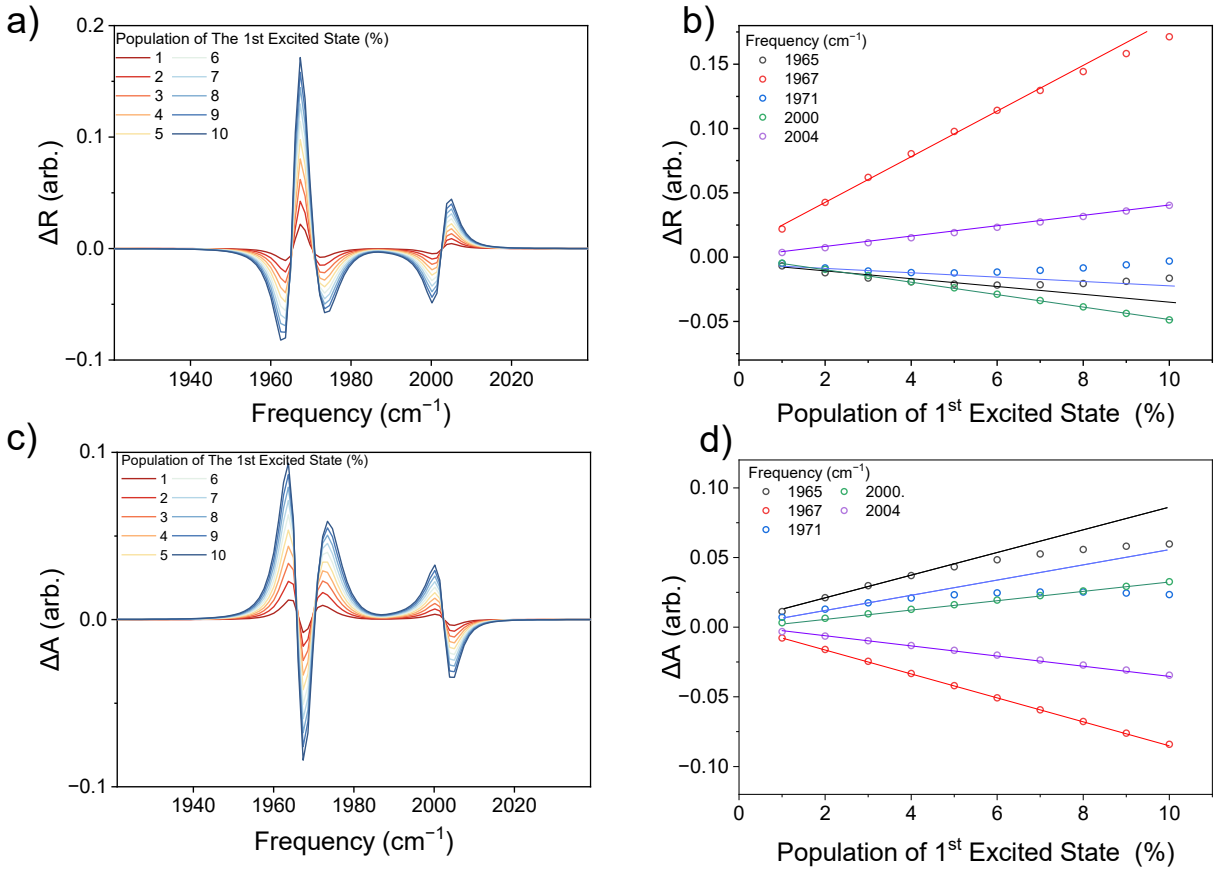

Figure 2. Simulated pump-probe reflection and absorption spectra of a Lorentzian oscillator with ground-state frequency of 1983 cm^{-1} that is coupled to the cavity mode. (a) Pump probe reflection spectra of a three-level system with the excited state absorption of 2←1 at 1968 cm^{-1}. (b) Population dependence of the signal intensities at given frequencies for (a). (c) Pump probe absorption spectra of a three-level system with the excited state absorption of 2←1 at 1968 cm^{-1}. (d) Population dependence of the signal intensities at given frequencies for (c).

Alternatively, global fitting,[30] a method widely adopted in transient absorption spectroscopy[35-40] to accurately extract kinetics has not been implemented for polariton studies, due to the challenges of non-intuitive correspondence between spectra and states, and the nonlinear population-spectral signal relationship as shown in Figure 1f.

In this article, we address these issues by developing a model of global fitting that describes the transient spectra using the first and second order perturbative expansions, i.e. Hessian. To elucidate

complexity the nonlinear correspondence issue, we employ numerical simulations to show that the nonlinear behavior originates from the second derivatives of the polariton signals with respect to excited-state populations, i.e. the Hessian term. We thereby introduced a second-order kinetic model by including the Hessian to describe the transient spectra. This model accommodates the nonlinear characteristics. Furthermore, it provides a robust framework for accurately extracting rate constants and identifying the species spectra associated with the corresponding excited states through global fitting, without the need of fitting each pump-probe spectra using TMM.

Theory

Experimentally, the pump-probe transmission spectra are recorded as the difference between the transmission spectra of the sample with and without pump excitation. The differential signal ΔT(ω, t), dependent on frequency (ω) and time (t), is represented by

$$\Delta T(\omega, t) = TMM\big(\omega, \boldsymbol{A}(t)\big) - TMM\big(\omega, \boldsymbol{A}(t=0)\big), \quad (1)$$

$$L_i(\omega) = A_i e^{-i\omega t}/(\omega_i^2 - \omega^2 - i\omega\Gamma_i), \qquad (2)$$

Where $TMM(\omega, \boldsymbol{A}(t))$ is the function derived from TMM to compute the polariton transmission spectra. Here, $\boldsymbol{A}(t)$ = (A_1(t), A_2(t)) are the amplitudes of transition for 2←1 and 3←2 anharmonic transitions described by Lorentzian functions (equation 2, where A_i is the amplitude, ω_i is the center frequency and Γ_i is the linewidth), which are proportional to the population of the corresponding excited states at time t. In general, $\Delta T(\omega, t)$ can be effectively expanded into a Taylor series with respect to the amplitude vector $\boldsymbol{A}(t)$, as shown in equation (3).[41]

$$\Delta T(\omega, t) = \left.\frac{\partial TMM}{\partial A_1}\right|_{t=0} A_1(t) + \left.\frac{\partial TMM}{\partial A_2}\right|_{t=0} A_2(t) + \frac{1}{2}\boldsymbol{A^T}(t)\boldsymbol{H}\boldsymbol{A}(t) \ldots\ldots \quad (3)$$

where $\boldsymbol{H}$ is the Hessian matrix.[41]

$$\boldsymbol{H} = \begin{bmatrix} \left.\frac{\partial^2 TMM}{\partial A_1^2}\right|_{t=0} & \left.\frac{\partial^2 TMM}{\partial A_1 \partial A_2}\right|_{t=0} \\ \left.\frac{\partial^2 TMM}{\partial A_2 \partial A_1}\right|_{t=0} & \left.\frac{\partial^2 TMM}{\partial A_2^2}\right|_{t=0} \end{bmatrix}, (4)$$

The $1 \leftarrow 0$ transition, or the ground state population, is not included as an independent variable, due to the conservation of total population. In most of ultrafast studies, this series can be truncated at the first order, e.g. $\left.\frac{\partial TMM}{\partial A_i}\right|_{t=0}$, suggesting a linear relationship between the transient spectra intensity and the corresponding excited state populations. However, as shown in Figure 1f, such a linear relationship breaks easily for the large absorptive (negative) feature in polariton transient spectra. Thus, we consider the second order in the expansion. Later, we will demonstrate numerically, this expansion is sufficient to address the nonlinear issue presented above, due to the typically small population of excited states induced by the finite pump fluence.

To validate the feasibility of the second-order Taylor expansion approximation, we simulated the pump-probe spectrum of a polariton formed by strong coupling the T_{1u} mode of C-O stretching in $W(CO)_6$ to the cavity mode[9] by subtracting the pump-on spectrum (with excited state transitions) from the pump-off spectrum (without excited state transitions), and used it as the 'ground truth'. The amplitudes, linewidths and the central frequency of the Lorentzian functions used to calculate the 'ground truth' in Figure 3 are summarized in Table 1. The amplitude for the ground state transition was attained from fitting the experimental linear transmission spectrum to reach Rabi splitting of 38 cm^{-1} at zero detuning.

Table 1: Parameters of the Lorentzian Functions Used in the Study

Center Frequency (cm^{-1})	1983	1968	1953
Amplitude (cm^{-2})	2309	243	53
Linewidth (cm^{-1})	8	11	14

In Figure 3, we compare the ground truth to the outcome from Equation 2 under various approximations. We find that neglecting the second derivative contributions significantly overestimates the negative signal in the LP region (1960 cm^{-1} to 1970 cm^{-1}, Figure 2a). However, when including second derivatives, the approximated spectra align closely with ground truth (Figure 3b), validating the approximation of truncating at second order.

Yet not all elements of the Hessian matrix significantly impact the second-order corrections. Given that the pump excitation predominantly promotes the first excited state population rather than the second, elements concerning the population of the second excited state should show negligible effects. This observation is supported by the calculated spectra in Figure 3c, where the Hessian is approximated to be $\boldsymbol{H} = \begin{bmatrix} \frac{\partial^2 TMM}{\partial A_1^2}\Big|_{t=0} & 0 \\ 0 & 0 \end{bmatrix}$. In Figure 3c, the theoretical spectrum closely resembles the ground truth, with only the LP negative peak to be slightly smaller than the one of ground truth. Thus, the pump-probe signal for vibrational polaritons can be simplified to:

$$\Delta T(\omega, t) = \frac{\partial TMM}{\partial A_1}\Big|_{t=0} A_1(t) + \frac{\partial TMM}{\partial A_2}\Big|_{t=0} A_2(t) + \frac{1}{2} * \frac{\partial^2 TMM}{\partial A_1^2}\Big|_{t=0} A_1^2(t)\,, (5)$$

This simplification significantly streamlines the kinetic model for vibrational polaritons, as the second-order correction comprises only a single dynamic component.

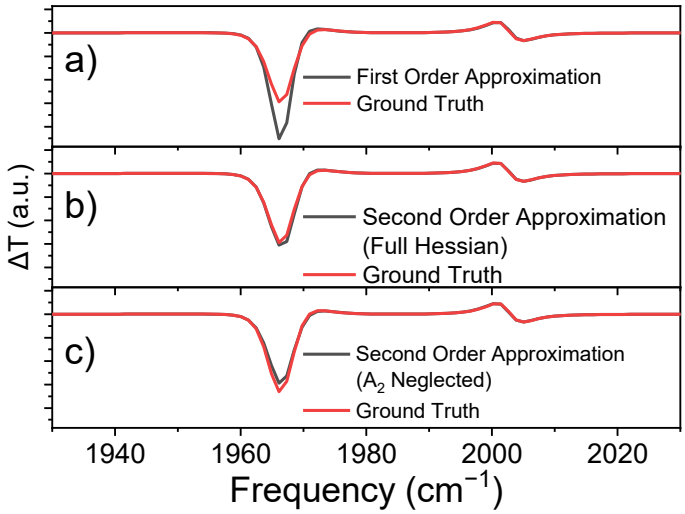

Figure 3: Comparison between the ground truth pump-probe spectrum and the approximated spectra calculated using equation 2. (a) only first order derivatives are included. (b) both first and second order derivatives are included. (c) only including $\frac{\partial^2 TMM}{\partial A_1^2}\Big|_{t=0}$ and the first order derivatives, which is enough to reproduce the ground truth.

Experimentally, the pump-probe data ΔT(ω, t) is captured as a two-dimensional matrix. The primary goal of the data analysis is to extract the dynamics of the intermediate states and the corresponding basis spectra in order to identify the intermediate states. Using $W(CO)_6$ as an example, the overall dynamics involves the relaxation of the first and second excited states,[42] which can be described by the following matrix equation:

$$\frac{d}{dt}\left[\begin{pmatrix} A_2 \\ A_1 \end{pmatrix}\right] = \begin{pmatrix} -k_2 & 0 \\ k_2 & -k_1 \end{pmatrix}\begin{pmatrix} A_2 \\ A_1 \end{pmatrix}, \qquad (6)$$

where k_1 and k_2 represent the relaxation rates of the first and second excited states, respectively. By incorporating second-order kinetics into our analysis, the kinetic model changes into the following:

$$\frac{d}{dt}\left[\begin{pmatrix} A_2 \\ A_1 \\ A_3 \end{pmatrix}\right] = \begin{pmatrix} -k_2 & 0 & 0 \\ k_2 & -k_1 & 0 \\ 0 & k_2A_2 - k_1A_1 & 0 \end{pmatrix}\begin{pmatrix} A_2 \\ A_1 \\ A_3 \end{pmatrix}, (7)$$

Here, we simply define $A_3 = {A_1}^2/2$ based on equation (5) and used the chain rule for derivatives.[41] We can obtain these relaxation rates from globally fitting the time-resolved spectra to our kinetic model. This fitting should not only produce the population dynamics but also the spectra associated with each state.

To validate specific kinetic processes further, we also need to compare the species-associated spectra with the derivative spectra $\frac{\partial TMM}{\partial A_1}\Big|_{t=0}$, $\frac{\partial TMM}{\partial A_2}\Big|_{t=0}$ and $\frac{\partial^2 TMM}{\partial A_1^2}\Big|_{t=0}$. This comparison is an approach to identify the corresponding states from the spectra. For example, according to Eq.(4), if one species spectrum resembles $\frac{\partial TMM}{\partial A_i}\Big|_{t=0}$, it indicates that state i is excited. Thus, it is necessary to calculate these derivative spectra as references.

Figure 4 presents the derivative spectra for the first and second excited states of a polariton system. Figure 4a clearly demonstrates that the second excited state spectrum ($\frac{\partial TMM}{\partial A_2}\Big|_{t=0}$) is red-shifted compared to the first excited state ($\frac{\partial TMM}{\partial A_1}\Big|_{t=0}$) and is characterized by a broader linewidth in the lower polariton (LP) region. Despite these differences, both states share a nearly identical line shape in the upper polariton (UP) region. This is reflective of the fact that the UP region is sensitive only to changes in the ground state population, while the LP region is affected by the excited state absorption (ESA).

Moreover, the second derivative spectrum ($\frac{\partial^2 TMM}{\partial A_1^2}\Big|_{t=0}$) of the first excited state exhibits a positive contribution to the LP region (Figure 4b). This observation is in line with calculations in Figure 3a, confirming that a first-order approximation would likely lead to an overestimation of LP intensity. In contrast, the second derivative spectrum exerts a negligible effect on the UP region. This agrees with that the UP region maintains a linear relationship between the signal and population, as concluded in Figure 1c. In the next sections, to validate and test the sensitivity of the global analysis method, two model data sets with different kinetics are produced by TMM which are analyzed globally with the second-order kinetic model.

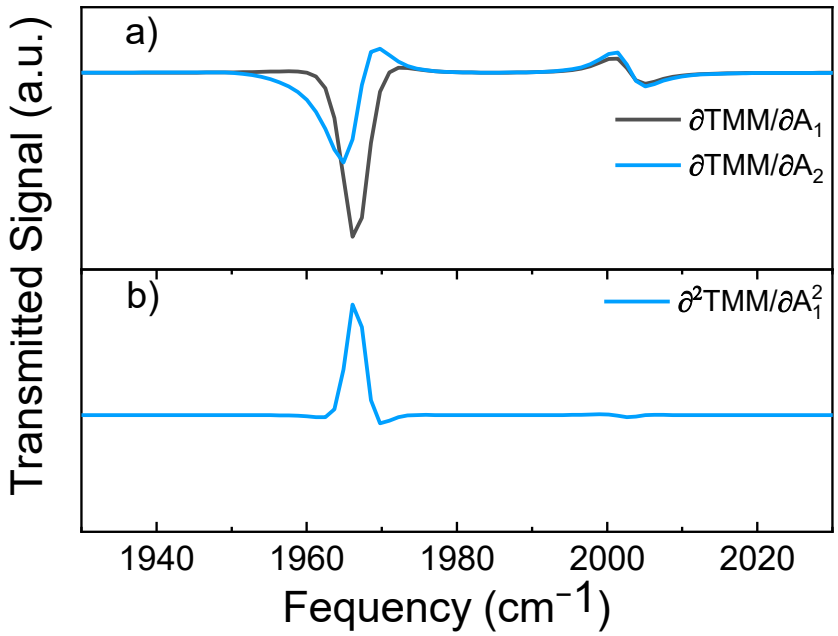

Figure 4: Derivative spectra calculated from TMM. (a) First and (b) second derivative spectra of the linear spectrum calculated by numerically differentiating the TMM equation with respect to the first and second excited state population.

Model 1. Vibrational relaxation of second and first excited states

Our first test model involves an ensemble of $W(CO)_6$ whose ground-state T_{1u} modes of C-O stretching are coupled to the cavity mode to reach VSC.[9, 23, 32] In our previous work, we showed spectral dynamic signatures that were attributed to the population of second excited states,[31] which were further supported by analytical theory[43] and numerical simulations.[44] Here we simulate this dynamics by describing it as that at time zero (t = 0), polariton instantaneously promote ten percent of the ground-state vibrations to the first and second excited states, whose characteristic relaxation rates remain the same as those of free-space $W(CO)_6$ molecules, which are $(70\ ps)^{-1}$ for the second excited state and $(140\ ps)^{-1}$ for the first excited state (Figure 5a).[9, 42] The pump-probe spectra from t = 0 ps to t = 250 ps are simulated using TMM, and the progression of the populations yields a series of pump-probe spectra at different time delays.

Figure 5b shows the 2D-contour of the pump-probe spectra and the spectral cut (normalized) in the early and late time to represent the spectral evolution. The ESA of first and second excited state is denoted by a prominent negative peak in the LP region, with the second-excited state's ESA broadening this peak, complicating the distinction from the first-excited state.

Performing the global fitting using the second-order kinetic model not only allows us to retrieve the rate constants accurately (Figure 5c and d), we obtained $(69.7\ ps)^{-1}$ and $(139.9\ ps)^{-1}$ for the second and first excited state relaxations respectively. The component spectra reach good agreement with the calculated derivative spectra: the first species (Species 1 in Figure 5d) shows a broad and red shifted peak in the LP region, which agrees with the $\frac{\partial TMM}{\partial A_2}\Big|_{t=0}$ spectra (black dots), indicating this spectral feature represents the 2nd excited state; in contrast, the second species (Species 2) is narrow and blue shifted, agreeing with characters of the $\frac{\partial TMM}{\partial A_1}\Big|_{t=0}$ spectrum (red dots). Thus, its dynamics describe the first excited state. It is noticeable that a discrepancy is

presented on the UP spectral side between Species 1 and its ground truth $\left.\frac{\partial TMM}{\partial A_2}\right|_{t=0}$. This is because the negligence of Hessian terms of A_2, i.e. $\left.\frac{\partial^2 TMM}{\partial A_2^2}\right|_{t=0}$ in the global fitting model. As a result, it reduces the bleach at LP side of the Species 1 spectrum, making the derivative spectra on the UP side larger than the ground truth after the spectrum being normalized to the bleach peak at LP region. It is worth noting that, while the kinetic model did not a priori identify the two states, this

information is attained from the species-associated spectra.

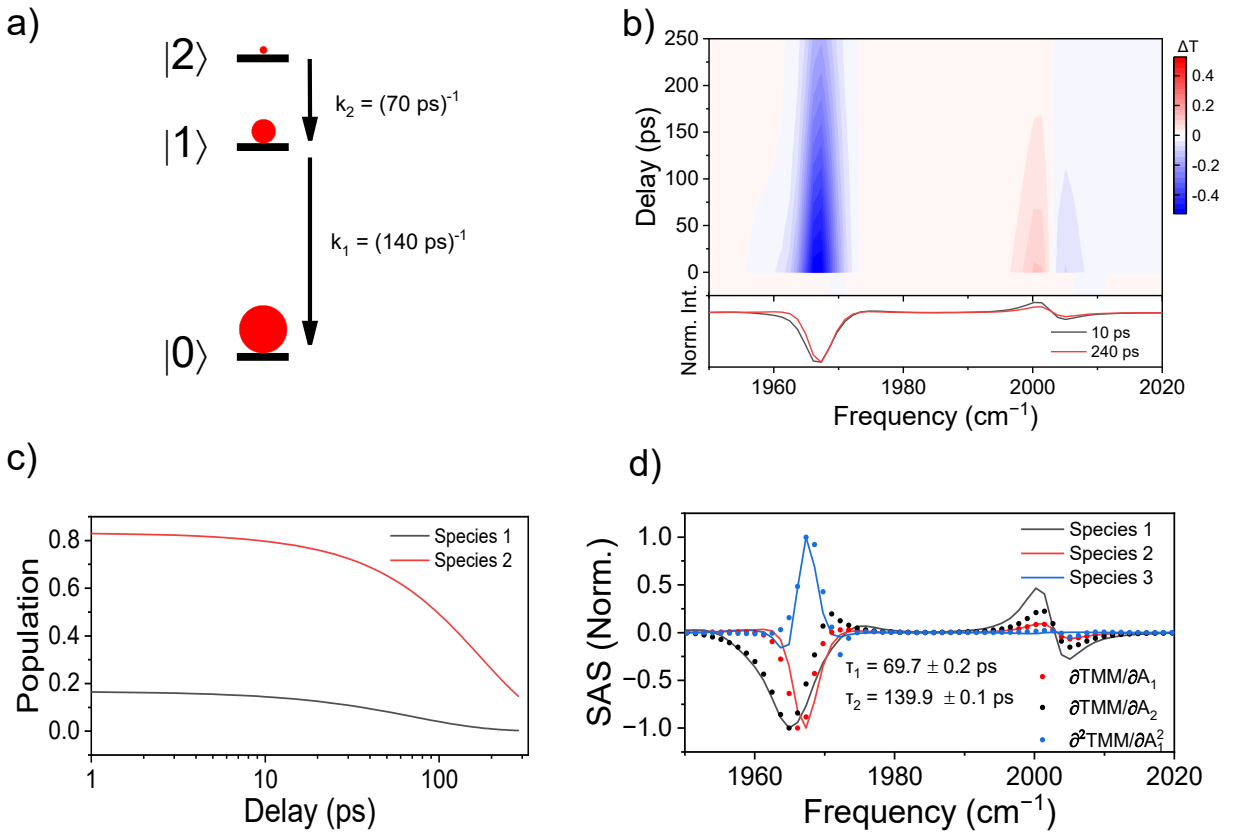

Figure 5: A sequential relaxation model. (a) Jablonski diagram describing the vibrational relaxation of the model. |0>, |1> and |2> are the ground state, first and second excited state of the vibration respectively. (b) Modeled pump-probe spectra of vibrational polariton that involves relaxation of first and second excited vibrational states of the molecular reservoir. Early and late time normalized spectral cuts are shown at the bottom. (c) The population dynamics of the species 1 and species 2. (d) Species spectra extracted from (b) using the second-order kinetic model. By comparing with derivatives of the linear spectra (dots), the specie spectra 1 and 2 can be related to the 2nd and 1st excited states respectively.

Model 2. Involvement of a Raman state in vibrational relaxation.

The second model involves population relaxation of a Raman state to the first excited states with the relaxation rate mirroring that of the second-excited states of the free-space $W(CO)_6$ molecules as described in Model 1 (Figure 6a). This is a mechanism our group recently proposed to explain

the early time dynamics of polariton systems.[34] This initial population of the Raman state can come from scattering of excited vibrational states with the aid of low frequency phonon or vibration modes, which was observed experimentally.[42, 45, 46]

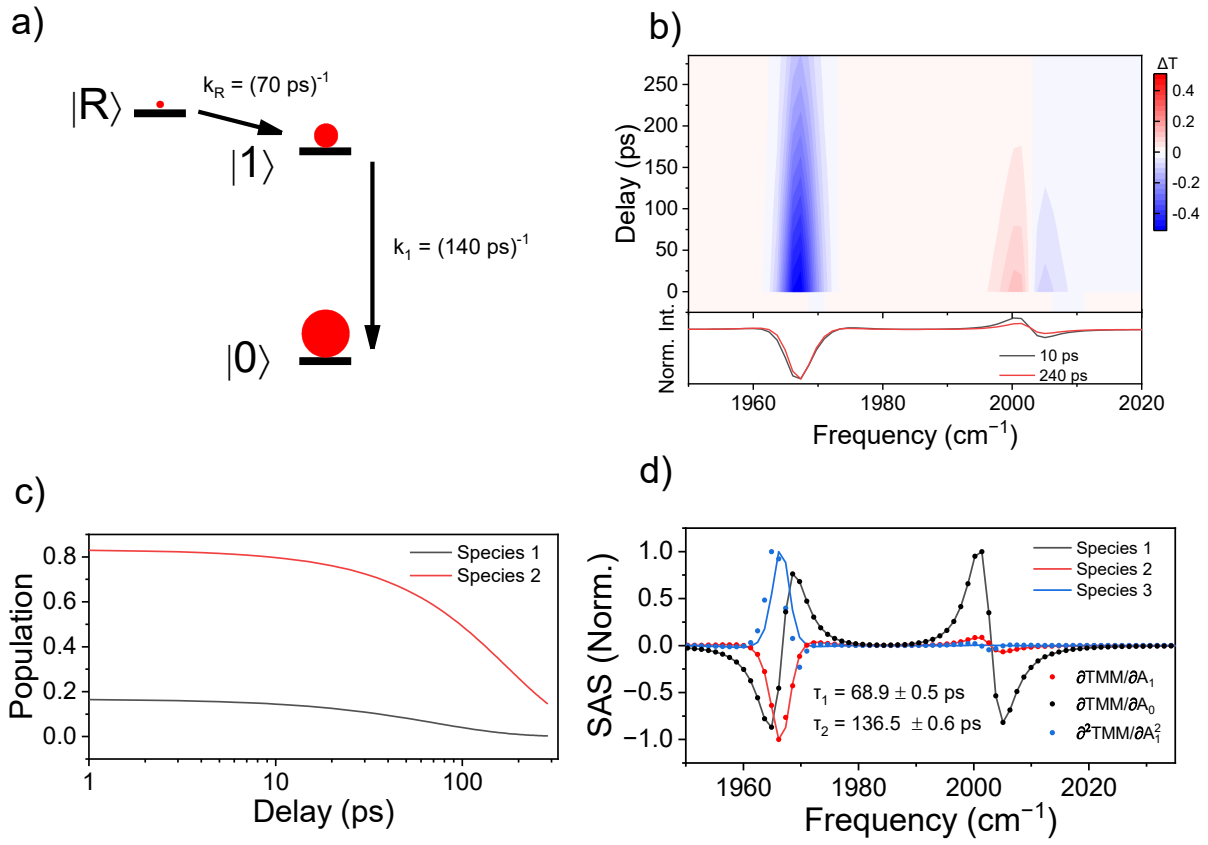

Figure 6: A polariton dynamic involving Raman states. (a) Jablonski diagram describing the vibrational relaxation of the model. |0>, |1> and |R> are the ground state, 1st excited state and the Raman state of the vibration. (b) respectively Model pump-probe spectra of vibrational polariton that involves relaxation of first excited vibrational state and the Raman state of the molecular reservoir, in which the Raman state population decays to the first excited state. Early and late time spectral cuts are shown at the bottom. (c) The population dynamics of the species 1 and species 2. (d) The species spectra extracted from (b) using the second-order kinetic model. Specie 1 spectrum exhibits double derivative features, agreeing with the initial Raman population in the model.

Due to the presence of an inversion center of $W(CO)_6$, no vibrational modes in the $W(CO)_6$ molecule can be both Raman and IR active, preventing the population of the Raman state from

being probed by directly by IR spectroscopy. However, population conservation indicates that the Raman population results in the reduction of the ground state population, which can cause Rabi splitting contraction. As a result, the first derivative spectrum arises from the Raman population in polaritons only contains a pair of derivative features (like Figure 6b), which is different from that of the first or second excited states. As seen in Figure 6b, the simulated spectral dynamics appear to be very similar to the one of Model 1 (Figure 5a). However, the LP region of the early and late time pump-probe spectra looks almost identical, making it hard to assign the intermediate state. In contrast, the species associated spectra in Figure 6d clearly shows species 1 as the derivative of a Lorentzian at both UP and LP regions, indicating the first intermediate state comes from an IR inactive population, which can be a Raman state. Species 2 and 3 exhibit the signature large bleach and positive signals respectively, matching the $\frac{\partial TMM}{\partial A_1}\Big|_{t=0}$ and $\frac{\partial^2 TMM}{\partial A_1^2}\Big|_{t=0}$ respectively, indicating the dynamics of species 2 reflect the one of first excited state. Notably, the population dynamics were accurately extracted (Figure 6c), agreeing the fact that Model 2 and 1 have the same dynamic rate, with the only difference to be the initial excited states which relax and populate the first excited and ground states.

Experimental Data

Lastly, having numerically verified the accuracy of this method, we apply the second-order kinetic model to the experimental pump-probe spectra (Figure 7a) and compare the species spectra with the calculated derivative spectra by TMM. The experimental detail and the layout of the laser table was described previously.[47] Briefly, the sample consists of saturated $W(CO)_6$ in hexane solution inside a cavity that is assembled with a pair of distributed Bragg reflector with 92% reflectance at 5 μm wavelength, the cavity spacing is around 12 μm to reach zero detuning. The achieved Rabi

splitting is 38 cm^{-1}. The pump and probe beam have the same incident angle (~ 1°) to the norm of the cavity assembly.

Without any assumption of the identities of the intermediate states, the species spectra extracted from the raw data show clear resemblance to the derivative spectra of the first and second excited states (Figure 7b), as large negative peaks appear on the LP region. This result indicates that, without considering the coherent dynamics occurs during polariton lifetime (typically < 5 ps),[48, 49] the experimental pump-probe spectra of $W(CO)_6$ polariton can be explained by the response of molecular reservoir, whose second excited state decays to the first excited state with a rate constant of $(59.8\ ps)^{-1}$, and the first excited state decays to the ground state with rate constant of $(153\ ps)^{-1}$.[9, 42] Such an excitation of second excited states can be controlled by pump fluences. For example, at higher fluence the second excited states can be further populated while the opposite is true at lower fluence conditions. We note that the species spectra suggests that there is no Raman mode necessary to be involved to account the observed dynamics here, suggesting that at least the Raman population, should it be excited in the polariton systems, is too small to be noticed by this method. This missing of Raman population could be due to the mismatch between the energy gap of Raman-polariton and the relevant phonon modes. Future experiments involving direct probing of the Raman population are warranted to provide definitive evident of the involvement of Raman

states in polariton dynamics.

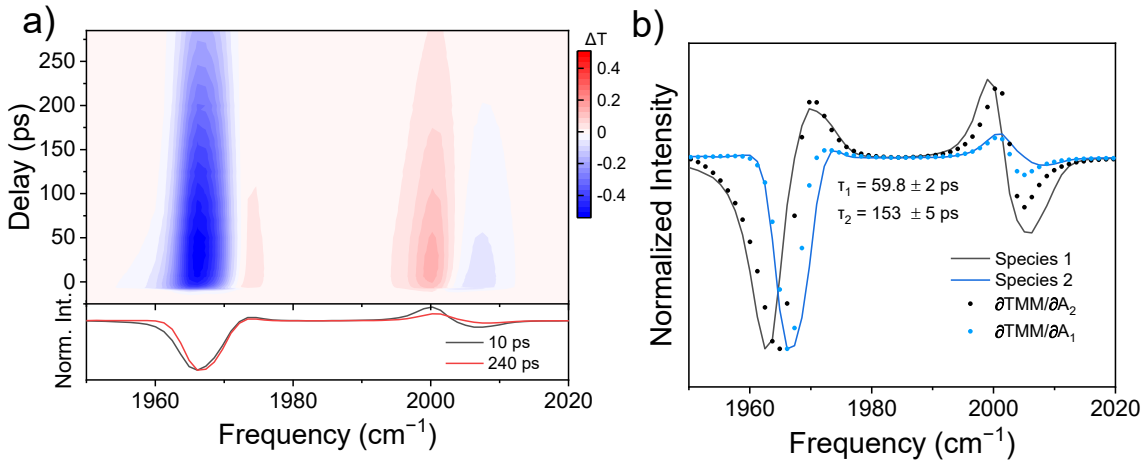

Figure 7: Experimental global analysis result. (a) Experimental pump-probe spectra of vibrational polariton that involves excited-state relaxation (b) The species spectra extracted from (a) using the second-order kinetic model. The deviation on the UP side (near 2000 cm^{-1}) between Species 1 and $\frac{\partial TMM}{\partial A_2}\Big|_{t=0}$ share the same origin of the one of Figure 4d.

Conclusion

We demonstrated the nonlinear signal-to-population relationship of pump-probe transmission spectra in the system with VSC and proposed a solution to the problem by expanding the TMM solution to its second order. The second order approximation allows us to derive the second-order kinetic equations, which can be used to globally fit the pump-probe data to extract both the rate constants and species-associated spectra. This approach can help identify the nature of the intermediate states associated with the kinetics through comparison with the calculated spectral derivatives. Although the two models used in this study involves up to 10% population of the excited states, such that the second-order approximation of the TMM equation can accurately capture the spectral feature, further expansion to higher orders is conceivable without additional parameters even if higher percentage of the excited-state population is present. However, because most of the samples of interest do not have as high of a nonlinearity as $W(CO)_6$, such that the

amount of population of the excited states fall into the linear signal-to-population regime, the use of conventional global analysis with first-order kinetic equations could become sufficient after validation of the linear relationship with the pump fluence. We note that the fitted dynamic constant should be accurate by itself regardless of the specific kinetic model being employed, whereas the accuracy of the extracted speciation spectra heavily relies on quality of the raw transient or 2D spectra. Thus, it requires caution to assign intermediates based on the extracted speciation spectra. The use of conventional global analysis would require an initial fitting of one single pump-probe spectrum at the early time delay to establish the excited state population's upper bound, followed by simulations to confirm linearity with decreasing populations, streamlining the kinetic analysis that addresses scientific questions that do not involve large amount of excited state population.

Reference

[1] J. P. Long, and B. S. Simpkins, ACS Photonics **2** (2015) 130.
[2] B. S. Simpkins, A. D. Dunkelberger, and I. Vurgaftman, Chemical Reviews **123** (2023) 5020.
[3] A. Shalabney *et al.*, Nature Communications **6** (2015) 5981.
[4] B. Xiang, and W. Xiong, Chemical Reviews **124** (2024) 2512.
[5] A. Thomas *et al.*, Angew. Chem. **128** (2016) 11634.
[6] A. Thomas *et al.*, Science **363** (2019) 615.
[7] F. J. Garcia-Vidal, C. Ciuti, and T. W. Ebbesen, Science **373** (2021) eabd0336.
[8] W. Ahn *et al.*, Science **380** (2023) 1165.
[9] A. D. Dunkelberger *et al.*, Nature Communications **7** (2016) 13504.
[10] A. B. Grafton *et al.*, Nature Communications **12** (2021) 214.
[11] G. Stemo *et al.*, The Journal of Physical Chemistry A **128** (2024) 1817.
[12] B. Xiang *et al.*, Science **368** (2020) 665.
[13] T.-T. Chen *et al.*, Science **378** (2022) 790.
[14] S. S. Demirchyan *et al.*, Physical Review Letters **112** (2014) 196403.
[15] Z. Yang, and W. Xiong, Advanced Quantum Technologies **5** (2022)
[16] A. Kavokin *et al.*, Nature Reviews Physics **4** (2022) 435.
[17] W. Ahn *et al.*, Science **380** (2023) 1165.
[18] A. Thomas *et al.*, Angew. Chem.-Int. Edit. **55** (2016) 11462.
[19] J. A. Hutchison *et al.*, Angew. Chem.-Int. Edit. **51** (2012) 1592.
[20] J. Lather *et al.*, Angew. Chem.-Int. Edit. **58** (2019) 10635.
[21] M. Du, and J. Yuen-Zhou, Physical Review Letters **128**, 096001 (2022) 7.
[22] T. Khazanov *et al.*, Chemical Physics Reviews **4** (2023)
[23] B. Xiang *et al.*, Proceedings of the National Academy of Sciences **115** (2018) 4845.
[24] B. Cohn *et al.*, J Chem Phys **159** (2023)
[25] S. Sufrin, B. Cohn, and L. Chuntonov, Nanophotonics **0** (2024)
[26] M. Son *et al.*, Nature Communications **13** (2022) 7305.
[27] L. Mewes *et al.*, Communications Physics **3** (2020) 157.
[28] F. Wu *et al.*, Nature Communications **13** (2022) 6864.
[29] W. Xiong, Acc. Chem. Res. **56** (2023) 776.
[30] C. Ruckebusch *et al.*, Journal of Photochemistry and Photobiology C: Photochemistry Reviews **13** (2012) 1.
[31] B. Xiang *et al.*, The Journal of Physical Chemistry A **123** (2019) 5918.
[32] A. D. Dunkelberger *et al.*, The Journal of Physical Chemistry A **122** (2018) 965.
[33] O. Hirschmann, H. H. Bhakta, and W. Xiong, Nanophotonics (2023)
[34] O. Hirschmann, H. H. Bhakta, and W. Xiong, Nanophotonics **13** (2024) 2029.
[35] B. K. Rugg *et al.*, Journal of the American Chemical Society **139** (2017) 15660.
[36] B. S. Basel *et al.*, Chem **4** (2018) 1092.
[37] M. C. Schwinn *et al.*, J Chem Phys **157** (2022) 184701.
[38] K. Zhang *et al.*, J Am Chem Soc **141** (2019) 17180.
[39] M. Chen *et al.*, Journal of the American Chemical Society **140** (2018) 9184.
[40] K. N. Schwarz *et al.*, Journal of the American Chemical Society **142** (2020) 2562.

[41] K. Binmore, and J. Davies, *Calculus : [concepts and methods]* (Cambridge University Press, Cambridge, 2007), 554 p. : ill.
[42] S. M. Arrivo *et al.*, Chemical Physics Letters **235** (1995) 247.
[43] R. F. Ribeiro *et al.*, Physical Review A **103** (2021)
[44] T. E. Li, A. Nitzan, and J. E. Subotnik, The Journal of Chemical Physics **154** (2021)
[45] A. Tokmakoff, B. Sauter, and M. D. Fayer, The Journal of Chemical Physics **100** (1994) 9035.
[46] A. Tokmakoff *et al.*, Chemical Physics Letters **221** (1994) 412.
[47] Z. Yang, H. H. Bhakta, and W. Xiong, Proceedings of the National Academy of Sciences **120** (2023) e2206062120.
[48] B. Xiang *et al.*, Science Advances **5** eaax5196.
[49] Z. Yang, B. Xiang, and W. Xiong, ACS Photonics **7** (2020) 919.

Acknowledgement

W. X. thanks Prof. Jinwei Hu from University of Washington for the insightful discussion. H.M. is supported by AFOSR Multidisciplinary University Research Initiatives (MURI) FA9550-22-1-0317, Awarded to W. X. W.X. acknowledge the general support from NSF DMR 1848215.

AUTHOR DECLARATIONS

Conflict of Interest

The authors have no conflicts to disclose.